Article

Chemosensor Development of Cu²⁺ Recognition Using 1,5-Diphenylthiocarbazone: Optimization, COSMO-RS and DFT Studies

Erna Normaya,   *, a Ros Syuhada,a Hakimah Ismail,a Mohammad N. Ahmad,a Mohd A. Yarmob and Ku H. K. Bulatc*

aExperimental and Theoretical Research Laboratory, Department of Chemistry, Kulliyyah of Science, International Islamic University Malaysia, 25200 Kuantan, Pahang, Malaysia

bSchool of Chemical Sciences and Food Technology, Faculty of Science and Technology, Universiti Kebangsaan Malaysia, 43600 Bangi, Selangor, Malaysia

cDepartment of Chemistry, Faculty of Science, Universiti Malaysia Terengganu, Mengabang Telipot, 21030 Kuala Terengganu, Terengganu Darul Iman, Malaysia

The sensitive and selective chemosensor for copper(II) ions (Cu²⁺) was successfully optimized using the 1,5-diphenylthiocarbazone (DPT) compound. The result showed that dimethyl sulfoxide (DMSO) in a 9:1 (DMSO:water) ratio at a pH of 3 was the optimum medium for DPT to act as chemosensor of Cu²⁺ recognition. The DPT chemosensor did not encounter any interference from other metal ions, including Fe^{3+}, Ag^+, Cr^{3+}, Pb^{2+}, Mg^{2+}, Cd^{2+}, Zn^{2+}, K^+, Ni^{2+} and Co^{2+}. The presence of Cu²⁺ led to an absorption peak at 658 nm, where the color changed from cantaloupe to gray-green color indicating the interaction by the formation of the DPT-Cu complex in 2:1 stoichiometry. The theoretical σ-profile calculation using conductor-like screening model for real solvents (COSMO-RS) showed the compatibility of DPT with the DMSO solvent through hydrogen bonding. In the density functional theory (DFT) calculations, the formation energy of DPT and DPT-Cu were −1113.79645660 and −2435.71832681 a.u., respectively. Under optimal conditions, a detection limit of 6.08 μM for the DPT chemosensor for Cu²⁺ recognition can compete with the flame atomic absorption spectroscopy (FAAS) value of 6.21 μM. Finally, DPT was able to provide less expensive, more portable and convenient chemosensor for Cu²⁺ recognition in environmental water samples.

Keywords: chemosensor, colorimetric, COSMO-RS, DFT, test strip

Introduction

Copper is a vital micronutrient for life and plays an important role in numerous essential reactions. Foods relatively high in copper content include mushrooms, dried fruits, legumes, whole-cereal grain products, peanut butter, nuts, organ meats (liver) and shellfish (crustaceans, oysters). Copper is essential for maintaining the strength of skin, blood vessels, epithelial and connective tissue throughout the body. Copper also plays an important role in the production of hemoglobin, myelin, melanin and it keeps thyroid gland functioning normally.[1] Copper deficiency may lead to anemia and bone marrow suppression, followed by a neurologic syndrome called myelopathy.[2] Copper can also act as a pro-oxidant that promotes free radicals, which may cause oxidative damage to lipids, proteins and DNA,

resulting in the development of neurodegenerative disorders such as Alzheimer's disease.[3] Detection of this metal ion is important because many industrial and agriculture activities release it into the environment. Copper can accumulate in soil and water, causing exposure to the food chain and aquatic life.[4] In typical environmental samples, it is difficult to detect metal ions due to the low concentration. Currently, the study of highly selective chemosensors for metal ion detection has attracted considerable attention.

Chemosensors are an alternative approach for the detection of metal ions within environmental and biomedical fields. Many existing methods for heavy metals detection, such as flame atomic absorption spectroscopy (FAAS) and inductive coupled plasma mass spectrometry (ICP-MS) are expensive, time-consuming and can only be used by skilled operator. Certain instruments cannot be used in the field for the rapid detection of unknown analytes because of the requirement of large or heavy instruments that require access

*e-mail: ernanormaya@gmail.com

to power outlets, solvents and chemicals. Alternatively, chemosensors utilize molecules that can bind selectively and reversibly with an anion or a cation.[5] Chemosensors offer several advantages, including the feasibility of naked-eye and on-site detection through color change in the presence of analytes. In addition, colorimetric chemosensors are an excellent alternative due to the low cost, as well as convenient and easy monitoring of the target ions.[6] The colorimetric chemosensor exploits the principles of ligand interactions with metal ion, leading to a change recognizable by the naked-eyes, which is very useful for this application.[7] The compound that was used in the chemosensor developed in this study was 1,5-diphenylthiocarbazone (DPT) (PubChem CID:657262), as shown in Figure 1. The sensitivity and selectivity of DPT to act as a chemosensor was optimized experimentally using UV-Vis spectroscopy.
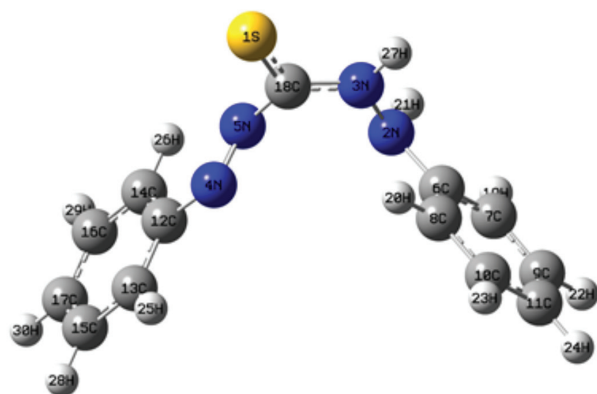

Figure 1. 3D structure of 1,5-diphenylthiocarbazone (DPT) (the nomination of the atoms in the image is inverted in relation to the text, but refers to the same atom).

The theoretical development approach used conductor-like screening model for real solvents (COSMO-RS) and density functional theory (DFT) calculations to thoroughly analyze the interaction and the chemical properties of DPT as a chemosensor for the Cu^{2+} recognition. COSMO-RS is a quantum chemical calculation-based simulation tool, which has been proven to precisely predict the chemical potential of a solute in aqueous and organic mixtures. DFT calculations are used to explain the molecular mechanism of the selective capture of metal ions by organic compounds and derivatives, as well as to determine the binding energy of ligand with metal ions.

Results and Discussion

Sensitivity optimization

Effect of solvents

Figure 2 shows the absorption spectra of DPT in different solvents in order to identify the most suitable solvent for interaction with DPT. The changes in the position of the peaks displayed by each solvent indicate the interaction of DPT with the solvent. Ethanol and acetonitrile displayed a band in a similar wavelength positioned at 420 nm. Since ethanol and acetonitrile were the most polar solvents, both were expected to be the most blue-shifted because hydrogen bonds form more readily at the ground state, thus increasing the energies of electronic transitions in the molecules.[8] The interaction with dimethylformamide (DMF) and dimethyl sulfoxide (DMSO) showed peak at 470 and 520 nm, respectively. These solvents were categorized as less polar solvents, thus resulting in higher wavelengths than for the polar solvents. DMSO was selected as the most suitable solvent based on the higher red-shifted absorption spectrum. This was due to the effect of the excited state dipole moment changes or changes in the hydrogen bonding strength of polar solvents.[5] Further explanation can be found in the "Theoretical studies" sub-section, regarding the interactions between each solvent and DPT using the COSMO-RS calculation.
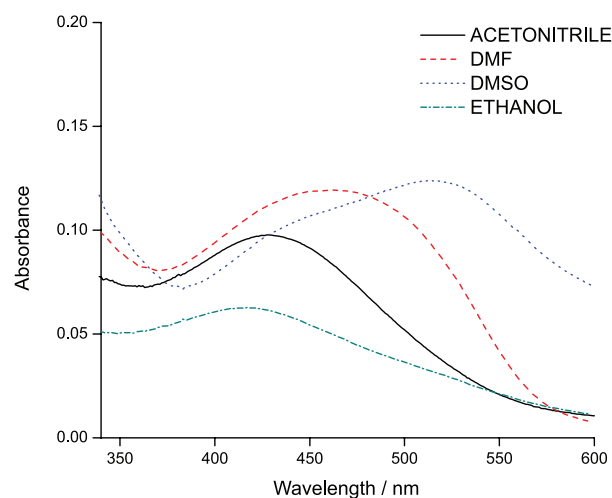

Figure 2. Absorption spectra of DPT (50 µM) in different solvents.

Effect of the co-solvent

Figure 3 shows the absorption spectra of DPT in DMSO and water mixtures with different solvent ratios *versus* the wavelength recorded for each reaction. Water was added as a co-solvent to increase the dielectric constant of the premier solvent, which resulted in increasing the sensitivity of the chemosensor. Based on the graph, there were two peaks observed at wavelengths of 450-490 and 620 nm, respectively. As the water volume fraction increased, the absorbance gradually decreased for both peaks.[9] The peak at 620 nm displayed a hypochromic effect, indicated by a decrease in the intensity of absorbance. The different DMSO:water

ratios provided different reactions during interaction with DPT. Referring to Figure 3, the 9:1 ratio was selected as the optimum and will be used throughout this study, due to exhibiting the highest hyperchromic effect, thus increasing the sensitivity of the chemosensor.[10]
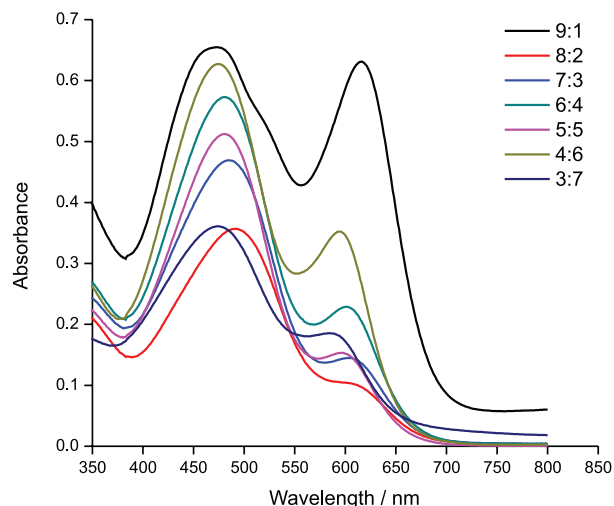

Figure 3. Absorption spectra of DPT (50 μM) for various DMSO:water ratios.

Effect of pH

Optimum pH was required to study the effect of different medium and conditions on the DPT sensor. The effect of the pH on the color intensity of the absorption spectra was studied. The pH values were prepared by combining specific amounts of citric acid and disodium phosphate solution using a pH meter. pH values from 1.0 to 7.0 were studied to optimize the chemosensor system, as shown in Figure 4. Based on the graph, the absorbance was observed to be constant and relatively unaffected at pH values of 1.0 and 2.0. The absorbance then increased to a maximum at a pH of 3.0 but decreased gradually from 4.0 to 7.0. A pH of 3.0 was chosen for further analysis because at this pH the color of the DPT-Cu complex showed stable absorption intensity, which indicated that Cu²⁺ could be clearly detected by the naked eye or UV-Vis measurement. This result showed that DPT and Cu²⁺ will favorably interact in an acidic medium, where DPT behaves as a monobasic acid in the complex formation.[11,12]
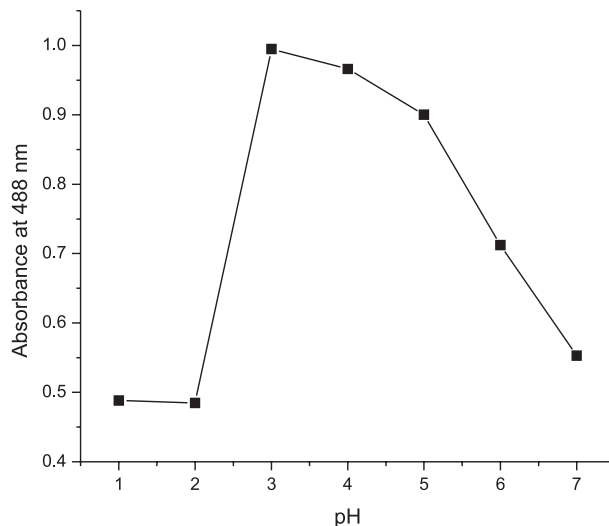

Figure 4. Absorbance of DPT (50 μM) for different pH at 488 nm.

Selectivity optimization

Naked eye observation

The selectivity of DPT in an optimized condition was conducted by testing 11 types of metal ions: Fe^{3+}, Ag^+, Cr^{3+}, Pb^{2+}, Cu^{2+}, Mg^{2+}, Cd^{2+}, Zn^{2+}, K^+, Ni^{2+} and Co^{2+}. The color of the DPT-Cu complex can be distinguished from the DPT-other-metal-ions by naked eye in Figure 5. This is an effective method for detecting Cu²⁺ ions from other metal ions by displaying an old moss green color while other metal ions showed no significant color change. The naked eye observation was supported by UV-Vis spectroscopy characterization in Figure 6, which confirmed that only DPT-Cu formed a new band at 658 nm. This indicated the formation of a new species (complex formation) with a molar extinction coefficient (ε) of 4×10^3 L mol⁻¹ cm⁻¹. The hypsochromic shift occurred from 500 to 488 nm. This blue shift was due to strong sulfur and nitrogen donor atoms binding to the Cu²⁺ ion. It also identified the shift to a shorter wavelength caused by the n-π* transition of sulfur chromophore.[10]

Interference analysis

Interference analysis was performed to study the selective affinity of DPT toward Cu²⁺ and to determine
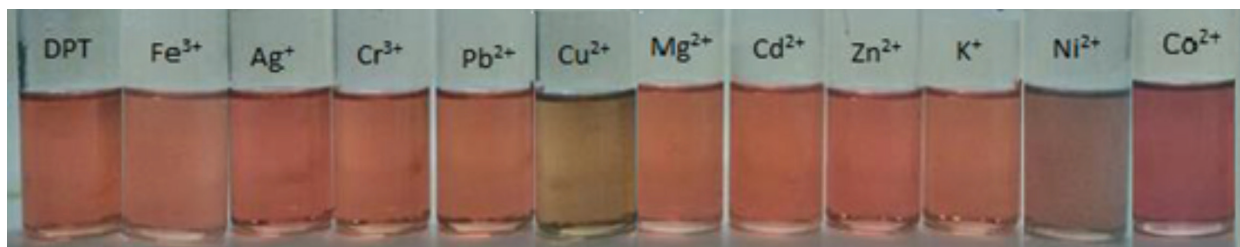

Figure 5. The observed color of DPT (50 μM) after the addition of metal cations under optimized conditions.
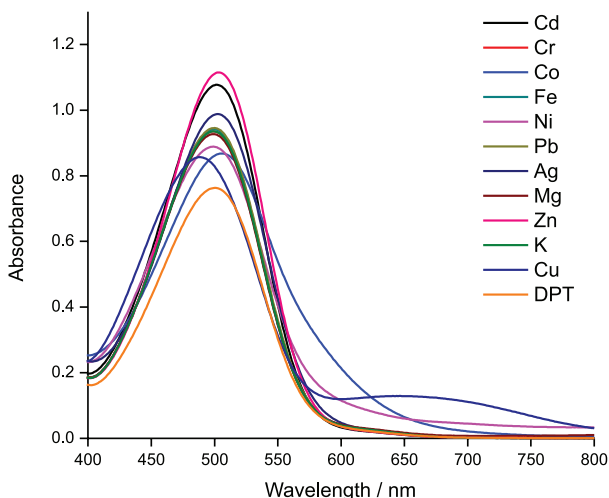
Figure 6. Absorption spectra of DPT (50 μM) with metal ions in a 9:1 ratio at pH 3.

the influence of other metal ions on the complex of DPT with Cu^{2+}. The presence of other metal ions (K^+, Cr^{3+}, Zn^{2+}, Cd^{2+}, Mg^{2+}, Ni^{2+} and Pb^{2+}) in different equivalents (1, 5 and 10) had showed no significant effect ($p \leq 0.05$) on the DPT-Cu complex except for Ag^+, Fe^{3+}, and Co^{2+} ions. As shown in Figure 7, the addition of different equivalents of other cations in the presence of Cu^{2+} also demonstrated higher absorbance than with DPT-cations alone. The result indicated that DPT could be used as a selective optical probe for detecting Cu^{2+} in presence of other competing metal ions.
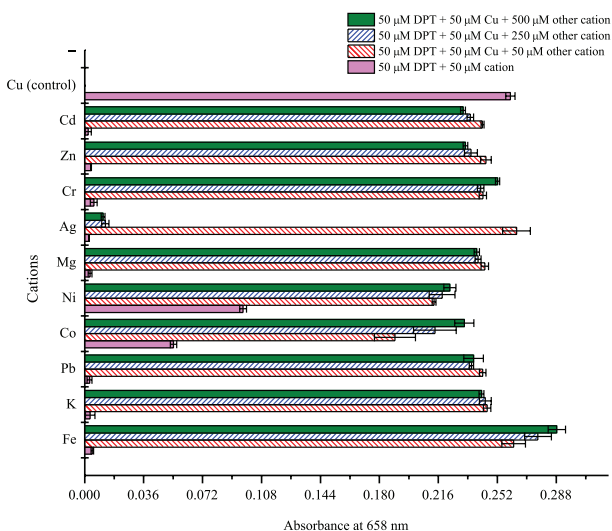

Figure 7. DPT selectivity against Cu^{2+} with different equivalents of other cations.

Limit of detection

A titration experiment was conducted using different concentration of Cu^{2+} in DPT under optimized conditions to study the effect of the concentration and to further analyze

the binding affinity of the sensor with Cu^{2+}. The titration experiment also determined the limit of detection of DPT for Cu^{2+} recognition. Figure 8 shows that upon the addition of different concentrations of Cu^{2+} to the DPT solution, a significant peak was observed at 658 nm with two clear isosbestic points at 390 and 570 nm. The distinct isosbestic points suggest that there was a total conversion of DPT into the DPT-Cu complex. It can be seen that the absorbance from 500 to 480 nm gradually decreased upon increasing the concentration of Cu^{2+}. In contrast, as the concentration of Cu^{2+} increased, the absorbance at 658 nm increased, indicating the complex formation also increased.
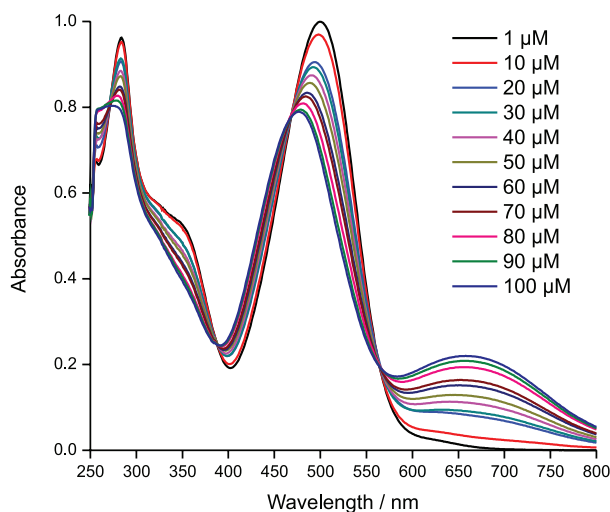

Figure 8. Absorption spectra of DPT (50 μM) with the addition of different concentration of Cu^{2+}.

The limit of detection is the lowest analyte concentration likely to be reliably distinguished from the blank and at which detection is feasible.[13] Replicates of the blank containing no analyte were tested and the limit of detection was calculated using the formula:

$$C_{DL} = 3\delta / K \qquad (1)$$

where δ is the standard deviation of the blank solution and K is the slope of the calibration curve.[14]

From the graph in Figure 9, the coefficient of determination (R^2) value was 0.9812, showing a good linear relationship between the absorbance and the concentration in the range of 1-100 μM of Cu^{2+}. From the calibration curve, the slope was 2.066×10^3 and the standard deviation value was 4.188×10^{-3}. The detection limit for Cu^{2+} using DPT was calculated to be 6.08×10^{-6} or 6.08 μM, which confirms that DPT can recognize Cu^{2+} with high sensitivity. The detection limit of the DPT probe and FAAS were compared and the calculation showed that the probe could compete with FAAS. The detection limits for DPT probe

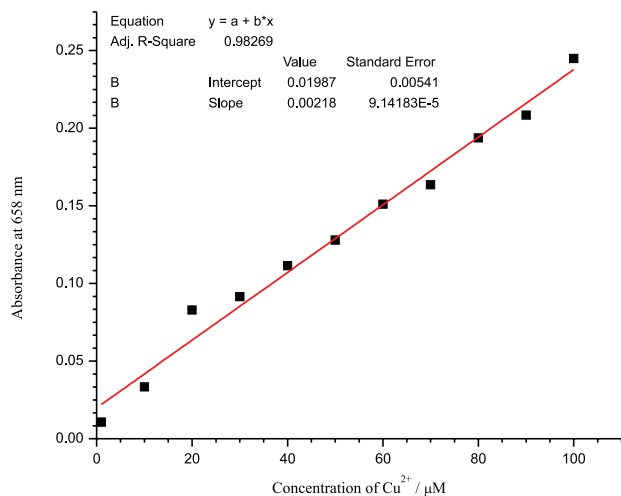and FAAS were 6.08 µM or 1.47 ppm and 6.21 µM or 1.50 ppm,[15] respectively.

Figure 9. Calibration curve for absorbance at 658 nm *versus* concentration of Cu^{2+}.

Job plot measurement

Stoichiometry of the DPT-Cu complex was determined by Job plot measurement. The Job plot was constructed by plotting absorbance *versus* mole fraction of Cu^{2+} at 658 nm, as in Figure 10. The binding stoichiometry between DPT and Cu^{2+} was represented by the mole fraction of the complex at maximum absorption. The maximum absorption intensity was observed at the 0.3 molar fraction. This indicated a 2:1 stoichiometry, which is the [L]/[Cu^{2+}] fraction between the DPT chemosensor and Cu.[16]
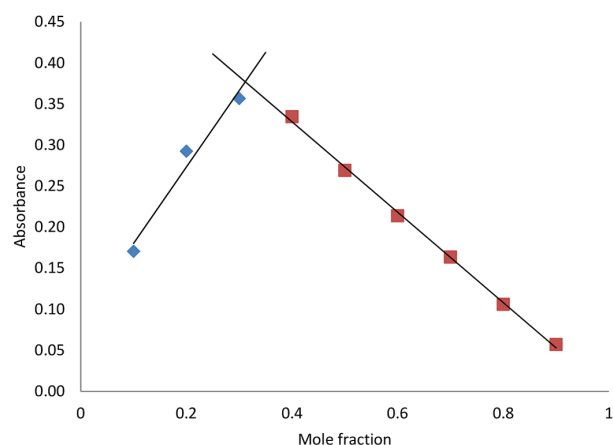

Figure 10. Job plot at 658 nm.

Colorimetric probe evaluation

The naked-eye detection analysis was conducted using test strips. Based on Figure 11, the color of test strips

under optimized conditions changed from cantaloupe (DPT only) to gray-green color on the cellulose paper, indicating the presence of Cu^{2+} ions in the lake water sample. It also showed that the Cu^{2+} ions were successfully bound with DPT and produced a significant color change. A further analysis using UV-Vis was conducted to evaluate the ability of DPT in acting as a chemosensor towards Cu^{2+} ions.
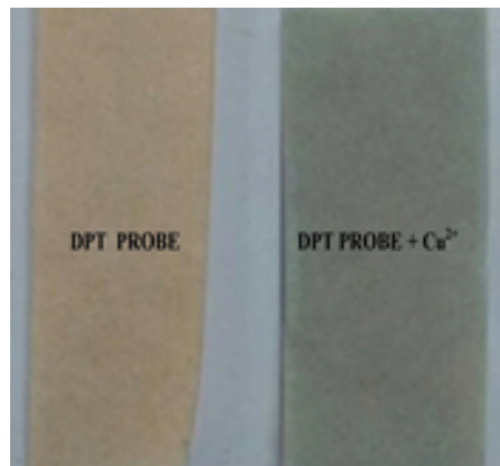

Figure 11. Color change of test strips for DPT and DPT + Cu^{2+} in the lake water sample.

UV-Vis analysis

The absorption response of Cu^{2+} ions (50 µM) with and without DPT (50 µM) in the lake water was conducted. As shown in Figure 12, a new band in the range of 600 to 800 nm was formed, showing that DPT can be used to detect Cu^{2+} in the lake water sample. The response from the absorption spectra was in good agreement to the results in Figure 11, indicating the feasibility of DPT for detecting Cu^{2+} in real environmental samples.
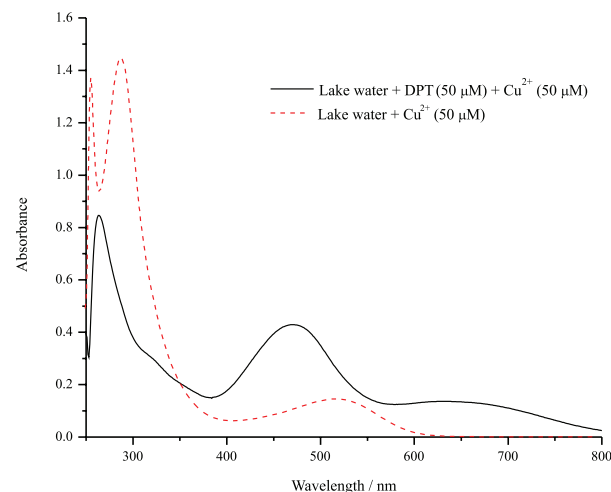

Figure 12. UV-Vis detection of Cu^{2+} ions in the lake water.

Validation of the model

The ability of DPT to act as a chemosensor also was validated using ICP-MS. The result showed that the concentration of Cu^{2+} ions in the lake water using UV-Vis analysis in presence of DPT as a chemosensor and ICP-MS were 51.750 ± 0.023 and 51.152 ± 0.008 µM, respectively. Tukey's test was done to validate both methods. It shows that, the new method development using UV-Vis in presence of DPT has no significant difference ($p \leq 0.05$) between the ICP-MS, which means the chemosensor by using DPT can be used as an alternative probe for detecting Cu^{2+} ions in environmental water samples.

Theoretical studies

σ-Profile analysis using COSMO-RS

In order to study the behavior of molecules in a solvent and the effect of functional grouping on electronic properties, a σ-profile of the molecule was constructed as in Figure 13. The σ-profile is defined as the probability distribution of surface charge density for a given molecule.[17] The σ-profile is related to the interaction of hydrogen bonds that determine the ability of hydrogen to act as a donor or acceptor. The main interaction that was favored by the DPT compound was polar interaction or hydrogen bonding. The molecules are considered polar when the screening charge density exceeds ± 0.008 e $Å^{-2}$. All σ-profiles of solvents had both polar and nonpolar sites on molecules. All solvents had a peak beyond $+0.008$ e $Å^{-2}$, which represented the presence of a hydrogen bond. Most solvents were located in the high polarity region ($\sigma > 0.008$ e $Å^{-2}$) and were considered to be hydrogen bond acceptors. The DPT compound and ethanol were observed at values below 0.008 e $Å^{-2}$, which act as hydrogen bond donors. DPT also showed a peak in the

H-bond acceptor regions, which indicates it could also act as a hydrogen bond acceptor. Other density distributions were observed around zero ($-0.008 < \sigma < 0.0085$ e $Å^{-2}$) and corresponded to non-polar groups of molecules. It was determined that all the solvents had the possibility to form hydrogen bonds with DPT compounds, because the DPT compound is a hydrogen bond donor. DMSO was selected as the most suitable solvent due to a similar σ-profile to DPT, as indicated by the compatibility of these two compounds. DMSO showed the highest absolute value of σ-profile and screening charge density, which leads to a stronger compound as a hydrogen bond acceptor.[18] The peak at the positive side of the DMSO σ-profile represented the increase in the hydrogen bond acceptor capability due to its oxygen atoms.[19] The negative side of the profile showed that DPT was dominated by blue regions, which are hydrogen bond donors.[18] This σ-profile shows the molecular polarization or interactions between the species.[20] The COSMO-RS calculation was also supported by the absorption spectrum in Figure 2, showing that DPT in DMSO solvent was red-shifted due to DPT and acted as a hydrogen donor while DMSO acted as a hydrogen acceptor in the studied medium.

Molecular electrostatic potential (MEP)

The correlation coefficient of the optimized geometry showed good agreement between calculated and experimental results, as shown in the Supplementary Information (Figure S1). The MEP of DPT was then calculated to visualize the electron distribution in the compound, as shown in Figure 14. MEP visualization is widely used as a reactivity map displaying the electrophilic and nucleophilic attack regions and to identify the potential regions available for the interaction to occur.[21] As shown in the figure, the regions of the S1, N5 and N4 showed
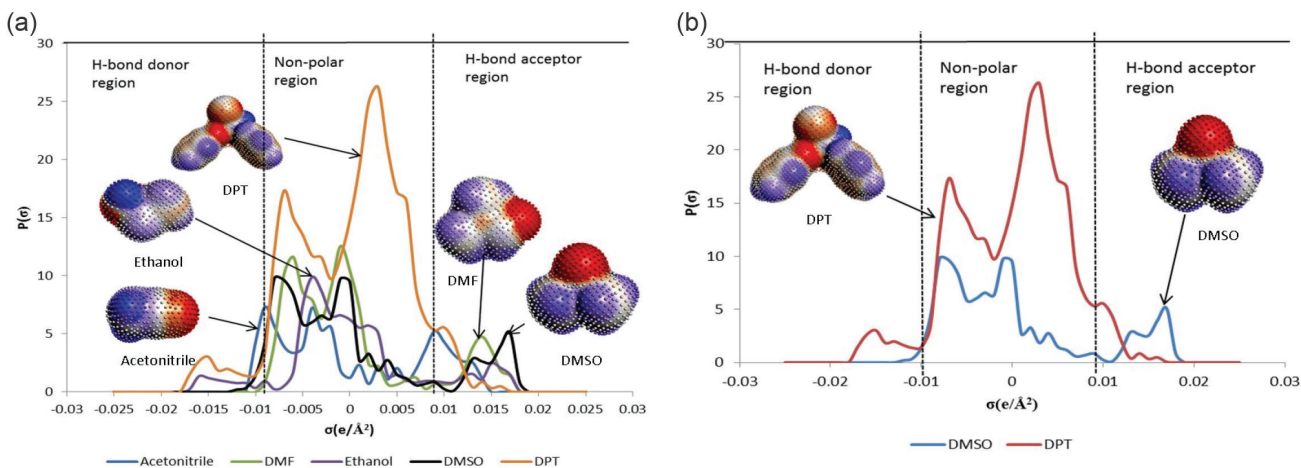

Figure 13. (a) σ-Profile of DPT and solvents used; (b) σ-profile of DPT and DMSO.

yellow region indicating the highest potential region for interaction with DPT-metal ion. There were also yellow regions around the phenyl rings due to the localization of electrons above and below the plane of the ring, making phenyl particularly stable.
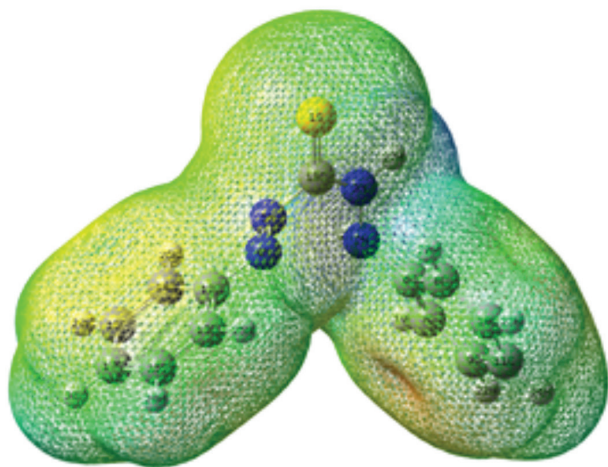

Figure 14. Molecular electrostatic potential of the DPT compound.

Fukui function

The Fukui function is a method in quantum chemistry to determine which atom is susceptible to nucleophilic or electrophilic attack (f_k^+, f_k^-, f_k^0). The calculation is based on the following equations:[22]

$$f_k^+ = [q(N + 1) - q(N)] \text{ for nucleophilic attack} \quad (2)$$
$$f_k^- = [q(N) - q(N - 1)] \text{ for electrophilic attack} \quad (3)$$
$$f_k^0 = 1 / 2[q(N + 1) - q(N - 1)] \text{ for radical attack} \quad (4)$$

where N, N − 1 and N + 1 are the total electrons present in the neutral, cationic and anionic states of the molecule, respectively. From the equations above, only the f_k^- was used to identify the atoms susceptible to electrophilic attack. The results are shown in Table 1.

The maximum value of the local descriptor susceptible to electrophilic attack was found to be S1 and N4 with values of 0.249 and 0.050, respectively (highlighted in bold). This is where the interaction is expected to occur, since S1 and N4 consist of high electron densities as compared to the other atoms in DPT. This allowed for the atoms to become nucleophilic and undergo a complex formation with the metal ion Cu²⁺.

HOMO-LUMO interactions

The MEP and Fukui function identified the region and the specific atom where the interaction occurred, thus HOMO-LUMO (highest occupied molecular orbital- lowest unoccupied molecular orbital) interactions were conducted

Table 1. Condensed Fukui minus functions using Mulliken charge analyses

Atom	Fukui function (f_k^-)
S1	**0.249**
N2	0.028
N3	0.008
N4	**0.050**
N5	0.039
C6	0.006
C7	0.024
C8	0.017
C9	0.019
C10	0.019
C11	0.033
C12	0.002
C13	0.010
C14	0.012
C15	0.016
C16	0.016
C17	0.022
C18	0.004
H19	0.039
H20	0.016
H21	0.037
H22	0.044
H23	0.040
H24	0.048
H25	0.024
H26	0.024
H27	0.046
H28	0.034
H29	0.037
H30	0.039

The maximum value of the local descriptor susceptible to electrophilic attack was highlighted in bold.

to analyze the formation energy and stability of DPT and DPT-Cu complexes. The energy levels of HOMO and LUMO are important in order to describe the reaction between compounds. HOMO is the orbital that acts as an electron donor, while LUMO is the orbital that acts as the electron acceptor. The 3D plots of selected molecular orbitals and the energy gap of each electronic transition are shown in Figure 15. Based on the figure, the HOMO and LUMO orbital of both the DPT and its complex were localized over S1, N−N bond and azo groups. The DPT compound underwent n-π* transitions, according to the visualization shown in the figure, which is in agreement with the blue shift reported in the solution spectra of Figure 6.
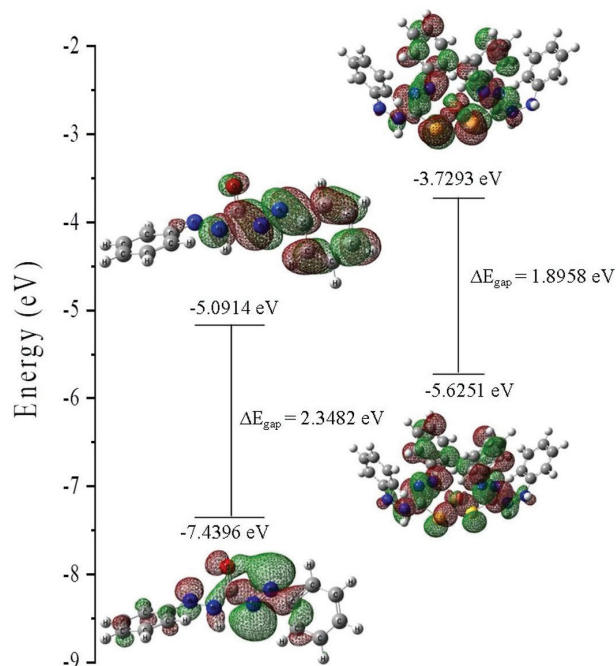
Figure 15. Energy level diagrams of HOMO and LUMO for (a) DPT and (b) DPT-Cu complex.

The interaction model of DPT and Cu^{2+} was constructed based on the Job plot measurement with 2:1 binding stoichiometry of the complex. For the formation of the complex, the energy gap of the frontier molecular orbital is at -1.8958 eV. This lower band gap energy indicates an easier combination of DPT binding with Cu^{2+} ions.[23] The transition occurred due to the complex formation of DPT with Cu^{2+} ions and resulted in the formation of new peak in the UV-Vis absorption spectra. The formation energy produced by the DPT was -1113.79645660 a.u., while the complex formation energy was calculated as -2435.71832681 a.u. The formation constant is a stability constant that measures the interaction between molecules during the formation of a complex. Generally, the energy will decrease during complex formation and the negative energy will result in the formation of a stable complex.[24] Thus, the higher negative energy produced in this study suggests that the DPT-Cu complex formed was thermodynamically stable.

Conclusions

In conclusion, the sensitivity optimization of DPT showed strong interaction with DMSO in a 9:1 (DMSO:water) ratio at a pH of 3. The sensor was selective for Cu^{2+} detection in aqueous solutions containing different metal ions. The detection limit of Cu^{2+} ion was as low as 6.08 µM. Job plots revealed that the sensor interacts with Cu^{2+} ions in the ratio of 2:1 stoichiometry. Computational calculations were used to support the binding mode

proposed between DPT and Cu^{2+} ion. The application of the probe using test strips was analyzed using lake water sample and successfully recognized Cu^{2+} ions by the color change. The validation method was also done to prove that DPT successfully acts as an alternative chemosensor for Cu^{2+} ions detection in environmental water sample. The probe is more affordable, portable and user-friendly, and it can also be used without any special training.

Experimental

Materials and instruments

All the chemicals and reagents were purchased from Sigma-Aldrich (United States of America), QRec (New Zealand), R&M Chemicals (Malaysia), HmbG Chemicals (Germany) and Bendosen (Malaysia). Absorption spectra were recorded at room temperature using a PerkinElmer model Lambda 35 UV/Vis spectrometer.

Sensitivity metal sensing analysis

The 50 µM DPT was dissolved in four different polarity solvents: DMSO, DMF, acetonitrile and ethanol. The DPT 50 µM with the selected solvent was prepared with different solvent:co-solvent (water) ratios (9:1, 8:2, 7:3, 6:4, 5:5, 4:6, 3:7, 2:8 and 1:9). The pH of the medium of DPT-Cu was prepared by combining appropriate amounts of specific chemical solutions under a pH meter. The UV-Vis spectrum of sensitivity optimizations was recorded over a wavelength range of 200-700 nm.

Selectivity metal sensing analysis

Under optimized conditions, the selectivity of DPT against a series of metal ions was determined. Each of the following metal ions with 1, 5 and 10 equivalents were added into 50 µM of DPT in the optimized solution: Fe^{3+}, Ag^+, Cr^{3+}, Pb^{2+}, Cu^{2+}, Mg^{2+}, Cd^{2+}, Zn^{2+}, K^+, Ni^{2+} and Co^{2+}. The selectivity of DPT (50 µM) for Cu^{2+} (50 µM) in the presence of other metals ions was then observed. Tukey's test was used to compare between the mean ± standard deviation using OriginPro software.[25]

Limit of detection

A titration method with variable Cu^{2+} concentration was conducted. Different concentrations of Cu^{2+} (1-100 µM) were added into the 50 µM of DPT under optimized conditions. A calibration curve of absorbance *versus* the concentration

of Cu^{2+} was constructed. The results obtained were used to determine the limit of detection using equation 1.

Job plot

A series of solutions containing DPT (50 µM) and Cu^{2+} (50 µM) were prepared in such a manner that the sum of the total Cu^{2+} and DPT volume remained constant (5 mL). Job plots were constructed at selected wavelength.

Probe validation

The test strips were immersed into a solution under optimized conditions and then dried under a vacuum condition. The probe was tested using spiked environmental water sample. The water sample was obtained from the International Islamic University Malaysia, Kuantan Campus and was digested using previous method.[26] Tukey's test was used to compare between the mean ± standard deviation using OriginPro software.[25] The result from UV-Vis analysis using DPT as a chemosensor was also compared with the ICP-MS by means of triplicate determination ($n = 3$) in order to determine the validity of the model. Results were considered statistically significant at $p \leq 0.05$.

Computational method

Optimization of the title compound and the solvents was the first step toward predicting the thermodynamic properties using COSMO-RS. The geometries and the continuum solvation COSMO calculations of solvent molecular surface density and the titled compound were optimized using DFT calculations with Becke-Perdew-86 (BP86) functional and triple zeta valance potential (TZVP) basis sets. After geometric optimization, the COSMO files containing the ideal screening charges on the molecular surface were generated and used to create the sigma profile and the polarity of the titled compounds. All the quantum calculations above were carried out using the Amsterdam Density Functional (ADF) program package, version 2017.[27] The DFT/B3LYP at the 6-311++G(d,p) basis set level using Gaussian09 program[28] was adopted to optimize geometrical parameters in the solution phase using the polarizable continuum model (PCM).[14] The 6-311++G (d,p) was chosen in order to obtain a suitable description of the polar bonds of the title compound. The d and p polarization functions on heavy atoms and hydrogen atoms were used, respectively. The most stable conformation (lowest total energy) was from the final optimization calculation for all theoretical considerations,

including the MEP, Fukui function and HOMO-LUMO energy calculations. The GaussView 5.0 program[29] was used to construct the optimized molecular geometry, MEP, HOMO and LUMO electron distributions and the HOMO-LUMO energy gap.

Supplementary Information

Supplementary information is available free of charge at http://jbcs.sbq.org.br as PDF file.

Acknowledgments

References

1. Osredkar, J.; Sustar, N.; *J. Clin. Toxicol.* **2011**, *S3*, 001.

2. Hedera, P.; Fink, J. K.; Bockenstedt, P. L.; Brewer, G. J.; *Arch. Neurol.* **2003**, *60*, 1303.

3. Gaetke, L. M.; Chow, C. K.; *Toxicology* **2003**, *189*, 147.

4. Nor, Y. M.; *Environ. Res.* **1987**, *43*, 274.

5. Orojloo, M.; Amani, S.; *Talanta* **2018**, *186*, 584.

6. Jang, H. J.; Ahn, H. M.; Kim, M. S.; Kim, C.; *Tetrahedron* **2017**, *73*, 6624.

7. Wasukan, N.; Srisung, S.; Kuno, M.; Kulthong, K.; Maniratanachote, R.; *Spectrochim. Acta, Part A* **2015**, *149*, 830.

8. Pavia, D. L.; Lampman, G. M.; Kriz, G. S.; Vyvyan, J. R.; *Introduction to Spectroscopy*, 4th ed.; Brooks/Cole: Belmont, 2010.

9. Wen, X.; Fan, Z.; *Sens. Actuators, B* **2017**, *247*, 655.

10. Li, Y.; Shi, W.; Ma, J.; Wang, X.; Kong, X.; Zhang, Y.; Feng, L.; Hui, Y.; Xie, Z.; *J. Photochem. Photobiol., A* **2017**, *338*, 1.

11. Bendix, G. H.; Grabenstetter, D.; *Ind. Eng. Chem.* **1943**, *15*, 649.

12. Irving, B. H.; Cooke, S. J. H.; Woodger, S. C.; Williams, R. J. P.; *J. Chem. Soc.* **1949**, *395*, 1847.

13. Armbruster, D. A.; Pry, T.; *Clin. Biochem. Rev.* **2008**, *29*, S49.

14. Sarkar, D.; Pramanik, A. K.; Mondal, T. K.; *Spectrochim. Acta, Part A* **2016**, *153*, 397.

15. PerkinElmer; *Atomic Spectroscopy: A Guide to Selecting the Appropriate Technique and System*; PerkinElmer: Waltham, 2008. Available at https://www.perkinelmer.com/Content/relatedmaterials/brochures/bro_worldleaderaaicpmsicpms.pdf, accessed in April 2019.

16. Likussar, W.; Boltz, D. F.; *Anal. Chem.* **1971**, *43*, 1265.

17. Roy, S.; Jaidann, M.; Ringuette, S.; Lussier, L. S.; Abou-Rachid, H.; *Procedia Comput. Sci.* **2010**, *1*, 1203.

18. Man, M. S.; Abdullah, M. A. M.; Abdullah, S. B.; Yaacob, Z.; *Indian J. Sci. Technol.* **2017**, *10*, DOI 10.17485/ijst/2017/v10i6/111218.

19. Rashid, Z.; Wilfred, C. D.; Gnanasundaram, N.; Arunagiri, A.; Murugesan, T.; *J. Mol. Liq.* **2018**, *255*, 492.

20. Jaapar, S. Z. S.; Morad, N. A.; Iwai, Y.; *J. Phys.: Conf. Ser.* **2013**, *423*, DOI 10.1088/1742-6596/423/1/012066.

21. Normaya, E.; Ahmad, M. N.; Farina, Y.; Bulat, K. H. K.; *J. Braz. Chem. Soc.* **2018**, *29*, 2197.

22. Parr, R. G.; Yang, W.; *Density-Functional Theory of Atoms and Molecules*, 1st ed.; Oxford University Press: New York, 1989.

23. Ding, X.; Zhang, F.; Bai, Y.; Zhao, J.; Chen, X.; Ge, M.; Sun, W.; *Tetrahedron Lett.* **2017**, *58*, 3868.

24. Qin, W.; Wang, J.; Xu, S.; Xie, Q.; Xu, Z.; *Colloids Surf., A* **2016**, *490*, 318.

25. *OriginPro*, version 2018 OriginLab Corp., Northampton, USA, 2018.

26. Abbasi, S.; Khani, H.; Tabaraki, R.; *Food Chem.* **2010**, *123*, 507.

27. Baerends, E. J.; Ziegler, T.; Atkins, A. J.; Autschbach, J.; Bashford, D.; Baseggio, O.; Bérces, A.; Bickelhaupt, F. M.; Bo, C.; Boerritger, P. M.; Cavallo, L.; Daul, C.; Chong, D. P.; Chulhai, D. V.; Deng, L.; Dickson, R. M.; Dieterich, J. M.; Ellis, D. E.; van Faassen, M.; Ghysels, A.; Giammona, A.; van Gisbergen, S. J. A.; Goez, A.; Götz, A. W.; Gusarov, S.; Harris, F. E.; van den Hoek, P.; Hu, Z.; Jacob, C. R.; Jacobsen, H.; Jensen, L.; Joubert, L.; Kaminski, J. W.; van Kessel, G.; König, C.; Kootstra, F.; Kovalenko, A.; Krykunov, M.; van Lenthe, E.; McCormack, D. A.; Michalak, A.; Mitoraj, M.; Morton, S. M.; Neugebauer, J.; Nicu, V. P.; Noodleman, L.; Osinga, V. P.; Patchkovskii, S.; Pavanello, M.; Peeples, C. A.; Philipsen, P. H. T.; Post, D.; Pye, C. C.; Ramanantoanina, H.; Ramos, P.; Ravenek, W.; Rodríguez, J. I.; Ros, P.; Rüger, R.; Schipper, P. R. T.; Schlüns, D.; van Schoot, H.; Schreckenbach, G.; Seldenthuis, J. S.; Seth, M.; Snijders, J. G.; Solà, M.; Stener, M.; Swart, M.; Swerhone, D.; te Velde, G.; Tognetti, V.; Vernooijs, P.; Versluis, L.; Visscher, L.; Visser, O.; Wang, F.; Wesolowski, T. A.; van Wezenbeek, E. M.; Wiesenekker, G.; Wolff, S. K.; Woo, T. K.; Yakovlev, A. L.; *ADF2017*; SCM, Theoretical Chemistry Department, Vrije Universiteit, Amsterdam, The Netherlands, 2017. Available at https://www.scm.com/product/adf/, accessed in April 2019.

28. Frisch, M. J.; Trucks, G. W.; Schlegel, H. B.; Scuseria, G. E.; Robb, M. A.; Cheeseman, J. R.; Scalmani, G.; Barone, V.; Petersson, G. A.; Nakatsuji, H.; Li, X.; Caricato, M.; Marenich, A.; Bloino, J.; Janesko, B. G.; Gomperts, R.; Mennucci, B.; Hratchian, H. P.; Ortiz, J. V.; Izmaylov, A. F.; Sonnenberg, J. L.; Williams-Young, D.; Ding, F.; Lipparini, F.; Egidi, F.; Goings, J.; Peng, B.; Petrone, A.; Henderson, T.; Ranasinghe, D.; Zakrzewski, V. G.; Gao, J.; Rega, N.; Zheng, G.; Liang, W.; Hada, M.; Ehara, M.; Toyota, K.; Fukuda, R.; Hasegawa, J.; Ishida, M.; Nakajima, T.; Honda, Y.; Kitao, O.; Nakai, H.; Vreven, T.; Throssell, K.; Montgomery Jr., J. A.; Peralta, J. E.; Ogliaro, F.; Bearpark, M.; Heyd, J. J.; Brothers, E.; Kudin, K. N.; Staroverov, V. N.; Keith, T.; Kobayashi, R.; Normand, J.; Raghavachari, K.; Rendell, A.; Burant, J. C.; Iyengar, J.; Tomasi, S. S.; Cossi, M.; Millam, J. M.; Klene, M.; Adamo, C.; Cammi, R.; Ochterski, J. W.; Martin, R. L.; Morokuma, K.; Farkas, O.; Foresman, J. B.; Fox, D. J.; *Gaussian 09, Revision E.01*; Gaussian, Inc., Wallingford, 2009.

29. Dennington, R.; Keith, T. A.; Millam, J. M.; *GaussView 5.0*; Semichem Inc., Shawnee Mission, KS, 2016.